Supplement of The Cryosphere, 19, 2935–2948, 2025
https://doi.org/10.5194/tc-19-2935-2025-supplement

The Cryosphere Open Access EGU

Supplement of

Impact of glacial isostatic adjustment on zones of potential grounding line persistence in the Ross Sea Embayment (Antarctica) since the Last Glacial Maximum

Samuel T. Kodama et al.

Correspondence to: Samuel T. Kodama (sakodama@ucsc.edu)

Contents of this file:

Text

Table

Figures

Supplementary Material

S1. Alternate Earth rheology model

To test the sensitivity of our results to the choice of Earth model, we simulate glacial isostatic adjustment W12 and Gol14 using an alternate Earth model characterized by a 50 km lithosphere and low viscosity zone of 10^{19} Pa·s from 50 km to 200 km depth, viscosity of 0.2 x 10^{21} Pa·s from 200 km to 670 km depth, and lower mantle viscosity of 3 x 10^{21} Pa·s. For the Gom18 ice history we explore sensitivity to Earth model by comparing to the 1-D reference Earth model, which has an upper mantle viscosity ~1-2 orders of magnitude higher than the 3D earth model (Gomez et al., 2018).

When we perform our grounding line persistence analysis using changes in topography simulated with the above alternate Earth models, we find broadly similar results, where zones of potential persistence migrate upstream from 20 ka to present day (Figure S7). With our alternate Earth model, there is a greater increase in "emergent" zones of potential persistence (zones that are only stable at present day and not at 20 ka) within the interior of the Ross Sea Embayment for all three ice histories, particularly for W12 and Gol14, as well as an increase in areas that are more stable at present day than at the last glacial maximum (red; Figure S7).

S2. Flowline modeling

To validate our simple model of grounding line persistence we run a 1-D marine ice sheet, shallow-shelf approximation, flowline model (Robel, 2021) over a representative ice stream path. We use a flowline model based off of the grounding line treatment from Schoof (2007) which has been benchmarked by modeling grounding line flux over a synthetic bed (Schoof 2007, Equation 10). Although the simple model of grounding line stability (main text) can efficiently test grounding line persistence for a large ensemble of parameters, it does not

account for ice flow aspects such as glacier velocity, ice thickness profiles, and interactions with upstream topography. The transient flowline model allows us to account for these variables and test if similar trends in grounding line behavior are observed in a more comprehensive model. Since the flowline model transiently evolves, a "stable steady-state" is not achieved, and we instead record trends in grounding line flux and retreat rate.

We test the impact of glacial isostatic adjustment-induced changes in topography on grounding line retreat by first solving for a steady-state ice profile with the grounding line located at the edge of the continental shelf, similar to the Last Glacial Maximum position of the flowline. The initial condition for the transient flowline run is a steady-state ice stream profile for both present-day (rebounded) and 20 ka (isostatically depressed) topographies. During the first timestep of the transient run, surface mass balance is step-decreased from 0.42 m/yr to -0.042 m/yr for all (present-day and 20 ka) model runs. Surface mass balance is then held constant at -0.042 m/yr for the remainder of the modeling time, and the model is run until the grounding line reaches the present-day grounding line position.

Input parameters of basal friction and ice shelf buttressing used for the flowline modeling are within the range of values used in the simple approximation used in the main text, while a higher initial average upstream surface mass balance (0.42 m/yr) was required to achieve a steady-state position on the edge of the continental shelf. Although the initial average upstream surface mass balance value is larger than the range of values used in the simple approximation used in the main text, the initial value and step change is the same for all modeling scenarios (present-day and 20), and therefore we can still isolate the role of glacial isostatic adjustment in grounding line retreat.

The ice stream flowline modeling results broadly agree with our analysis using the simple grounding line approximation in the main text. We interpret locations with smaller grounding line discharge and slower retreat rates as more "stable" (similar to our potential zones of persistence in the main text). The simple groundling line stability model (main text) predicts grounding line persistence for Gom18 paleo-bathymetry near the edge of the continental shelf (~1,600 km; Figure S2b) and near the present-day grounding line (~800 km; Figure S2b), and the ice stream flowline model produces the smallest grounding line retreat rates and grounding line discharges at these locations as well. A similar spatial pattern is seen with present-day bathymetry (black; Figure S2). The simple grounding line stability model also predicts a small number of potential stable steady-state grounding line zones for present-day bathymetry between 900–1,400 km downstream (Figure S2), but no potential stable grounding line zones over this reach for 20 ka paleo-bathymetries. Over the same reach, the flowline model produces grounding line retreat rates over present-day bathymetry that are ~5-10 times slower than those over 20 ka paleobathymetry.

S3. Emergent potential zones of grounding line persistence

We term, "emergent" zones of potential persistence as zones of potential persistence that are stable at present-day, but not stable at a specific previous time in the deglaciation (e.g. zones that are "emergent" at 15 ka are stable at present-day but not at 15 ka). For each time-step we calculate the number of "emergent" zones of potential persistence for that specific timestep. We

then normalize all times by dividing by the maximum number of "emergent" zones of potential persistence at a given timestep, which occurs at 12.5 ka for Gol14 and Gom18, and at 10 ka for W12.

The maximum number of "emergent" zones of potential persistence occurs 12.5-10 ka because this is the time of maximum relative sea level within the Ross Sea Embayment. The timing of the maximum relative sea level is a function of the timescale of local isostatic rebound and the timing of global sea-level rise. The Ross Sea Embayment reaches maximum isostatic depression ~20 ka. However, maximum relative sea-level within Ross Sea Embayment during the deglaciation occurs ~10-12.5 ka because the rate of global mean sea-level rise outpaces the rate of sea-level fall due to local isostatic uplift during the beginning of the deglaciation.

This interaction between near-field sea-level fall and global sea-level rise results in a maximum of relative sea-level ~10-12.5 ka and a minimum in zones of potential persistence due to the deep depths within the Ross Sea Embayment at these times. Therefore, 10-12.5 ka is the time with the least number of zones of potential persistence compared to the present-day and the greatest number of "emergent" zones of potential persistence.

A small area of emergent potential zones of grounding line persistence is located on a large submarine bank near the edge of the continental shelf (PB; Main text Figure 1e and Figure 3) despite this area undergoing a sea-level rise since 20 ka. At 20 ka, the depth of this bank is shoaled due to global sea-level fall and uplift of the peripheral bulge, such that we predict positive mass balance (resulting in grounding line advance) on this shoaled bank at 20 ka. Once relative sea level at the bank increases due to global sea-level rise and peripheral bulge collapse, fluxes out of the grounding line increase sufficiently to balance fluxes into the grounding line, producing stable steady-states. As a result, the 20 ka bathymetry contains no stable steady-state grounding line positions (due to ice sheet advance) and present-day bathymetry contains stable steady-state grounding line positions due to a cessation of this advance because of relative sea-level rise.

S4. Full derivation of Stable Grounding Line Equation for linear stability analysis

The original equation:

$$\frac{d}{dL}\left(PLh_g^{-1} - \Omega h_g^{\beta-1}\right) \tag{1}$$

Applying the chain rule to PLh_g^{-1}

$$Ph_g^{-1} - PL\frac{dh_g}{dL}h_g^{-2} \quad -\frac{d}{dL}\left(\ \Omega h_g^{\beta-1}\right) \tag{2}$$

Applying the chain rule to $\Omega h_g^{\beta-1}$

$$Ph_g^{-1} - PL\frac{dh_g}{dL}h_g^{-2} \quad -(\beta-1)\Omega h_g^{\beta-2}\frac{dh_g}{dL} \tag{3}$$

Applying that $h_g = -\frac{\rho_w}{\rho_i}b$, where b is a function of L

$$Ph_g^{-1} + \left[PLh_g^{-2} + (\beta-1)\Omega h_b^{\beta-2}\right]\frac{\rho_w}{\rho_i}\frac{db}{dL}$$

S5. Decomposition of relative sea level

To understand which processes are contributing to changes in relative sea level (RSL) within the Ross Sea Embayment we decompose two relative sea-level curves into changes caused by deformation of the solid Earth (R) and changes due to direct gravitational effect and global sea-level change (G). In Figure S3, we show RSL decompositions for the W12 and Gol14

ice histories at two locations: 1) within the interior of the Ross Sea Embayment and 2) near the edge of the continental shelf.

Near the edge of the continental shelf, RSL is predominantly caused by global sea level rise due to global ice sheet melt, which causes ~130 m of sea level rise. Peripheral bulge collapse only causes ~10 m of RSL rise, an order of magnitude smaller. However, these forcings occur at different times. RSL rise due to changes in global sea level occur primarily from 20-10 ka, while changes in RSL due to peripheral bulge collapse occur from 8 ka to present-day.

Within the interior of the Ross Sea Embayment RSL is predominantly caused by isostatic rebound due to local ice mass loss. Over the deglaciation isostatic rebound causes RSL fall of ~250 m, twice the magnitude of sea level rise caused by global sea-level rise. The relative timing of these two RSL forcings produces maximum RSL within the Ross Sea Embayment interior 10-12 ka. This timing is because even though the interior of the Ross Sea Embayment begins rebounding at 20 ka, inducing a sea-level fall, global sea-level rise outpaces the rate of isostatic rebound from 20 ka to 10-12 ka resulting in a net RSL rise. At 10-12.5 ka the rate of isostatic rebound outpaces the rates of global sea-level rise, leading to a transition to a net sea-level fall.

Supplementary Table

STable 1: Parameters used in Flowline modeling	
Parameter	Value
upstream average surface mass balance at t_0 ($\frac{m}{yr}$)	0.1
upstream average surface mass balance at $t_{1\rightarrow\infty}$ ($\frac{m}{yr}$)	0.03
Nye-Glen law coefficient ($Pa^{-n} \cdot s^{-1}$)	4.227 x 10^{-25}
Weertman friction law exponent	$\frac{1}{3}$
Nye-Glen law exponent	3
Basal friction coefficient ($Pa \cdot m^{\frac{-1}{n}} \cdot s^{\frac{1}{n}}$)	6 x 10^6
Ice shelf Buttressing parameter	0.5
Ice density ($\frac{kg}{m^3}$)	917
Sea water density ($\frac{kg}{m^3}$)	1028

Table S1 | Values of parameters used for flowline modeling.

Supplementary Figures

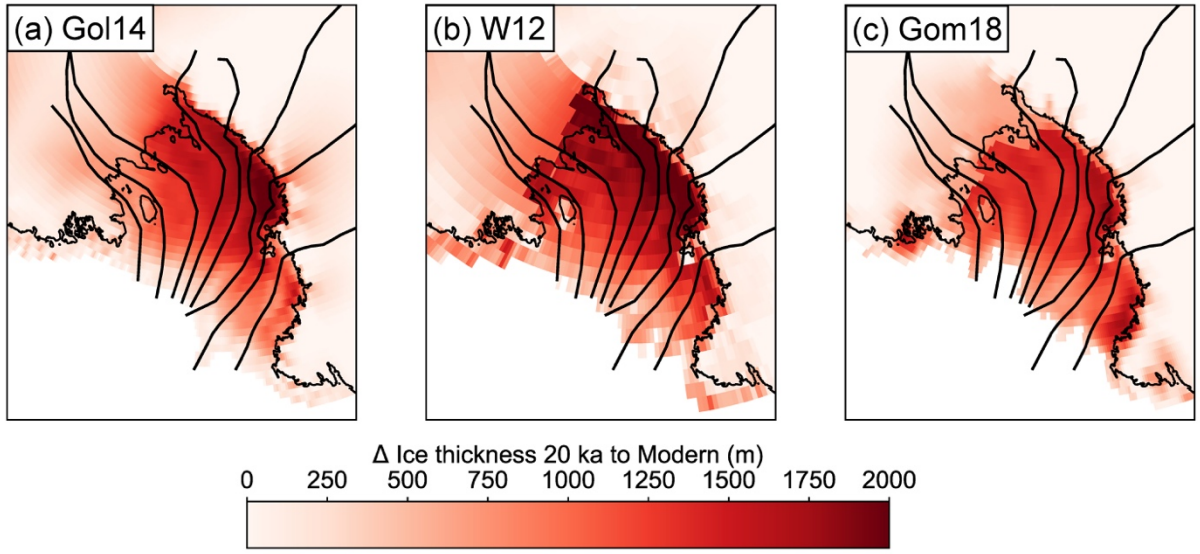

Figure S1 | Change in ice thickness since 20 ka in the Ross Sea for a) Gol14, b) W12, and c) Gom18 deglacial histories. Flowlines are the same as in the main text. This black line is present-day grounding line taken from MEaSUREs (Rignot et al., 2011).

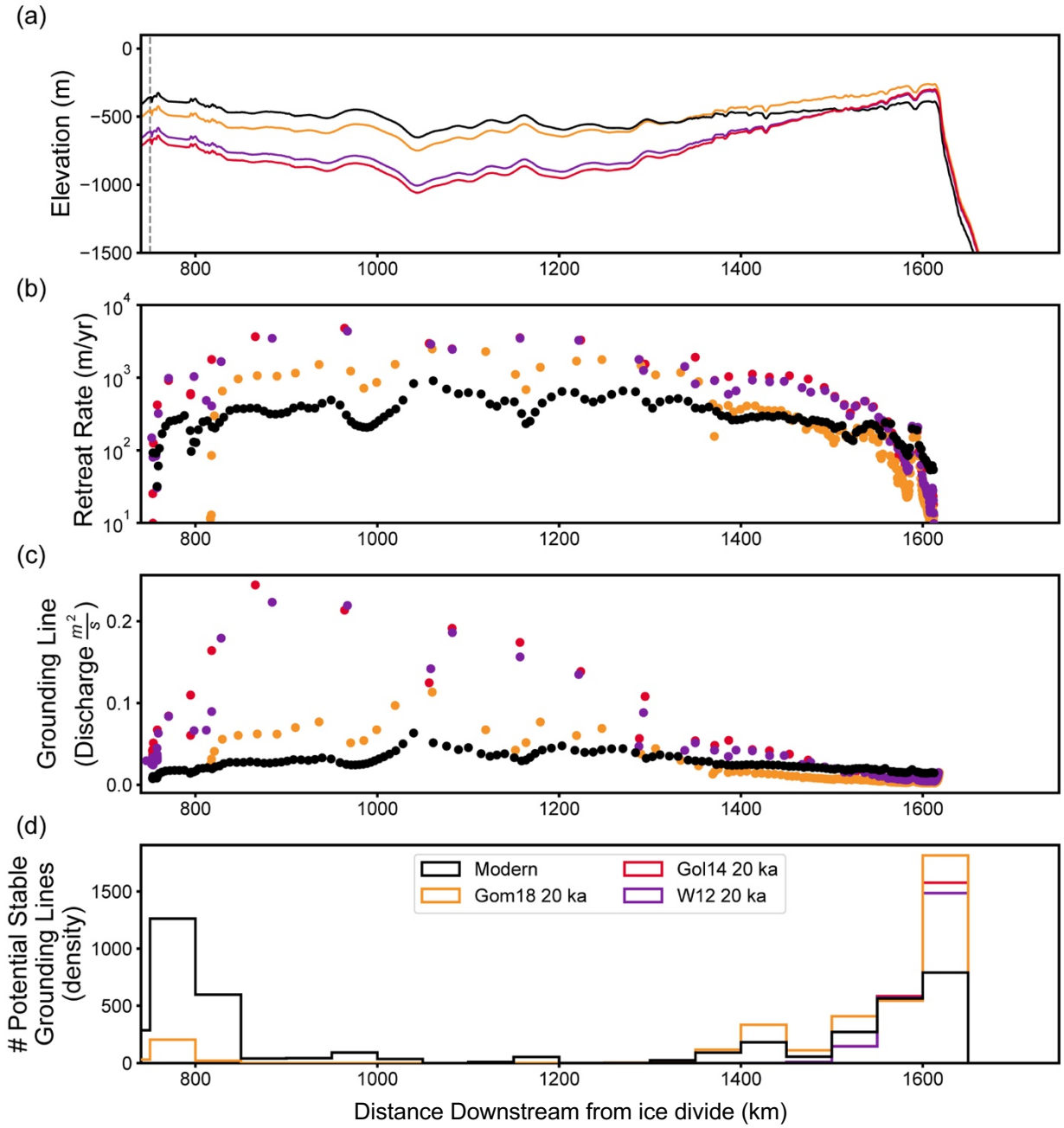

Figure S2 | a) Present-day topography (black), and 20 ka paleotopography modeled with W12 (purple), Gol14 (red), and Gom18 (orange). Dashed line is present-day grounding line location. b) Grounding line retreat rate, c) Grounding line discharge, and d) Potential stable grounding line positions simulated using the simple grounding line flux approach described in the main text.

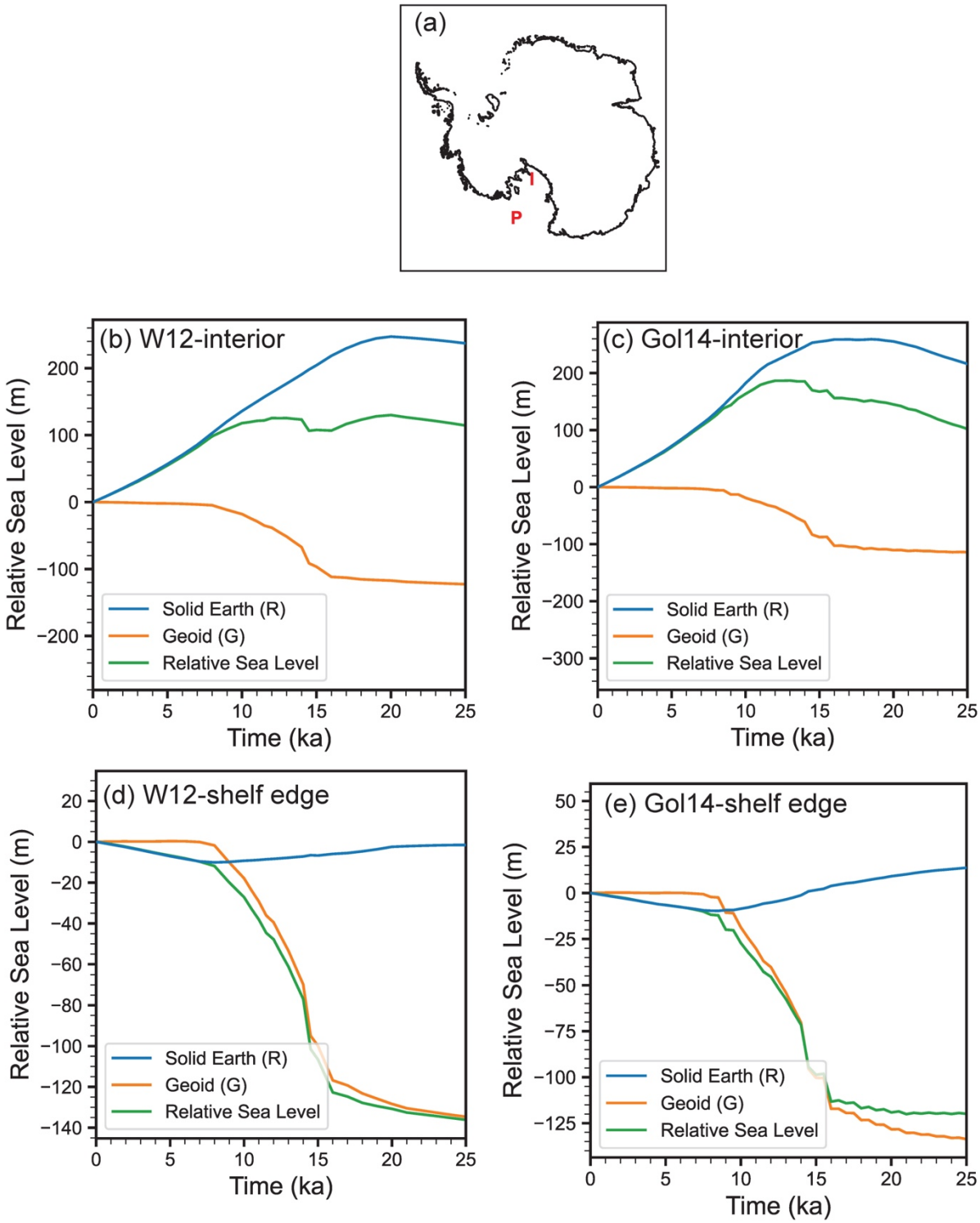

Figure S3 | Relative Sea Level (green) decomposed into solid Earth (R; blue) and geoid (G; including direct gravitational effect and global sea-level change; orange) components for a) Gol14 and b) W12 ice histories. a) Map of Antarctica showing location of relative sea-level curves for the interior (I) and shelf edge (P). b/d) Relative sea-level curves for W12 ice history. c/e) Relative sea-level curves for Gol14 ice history.

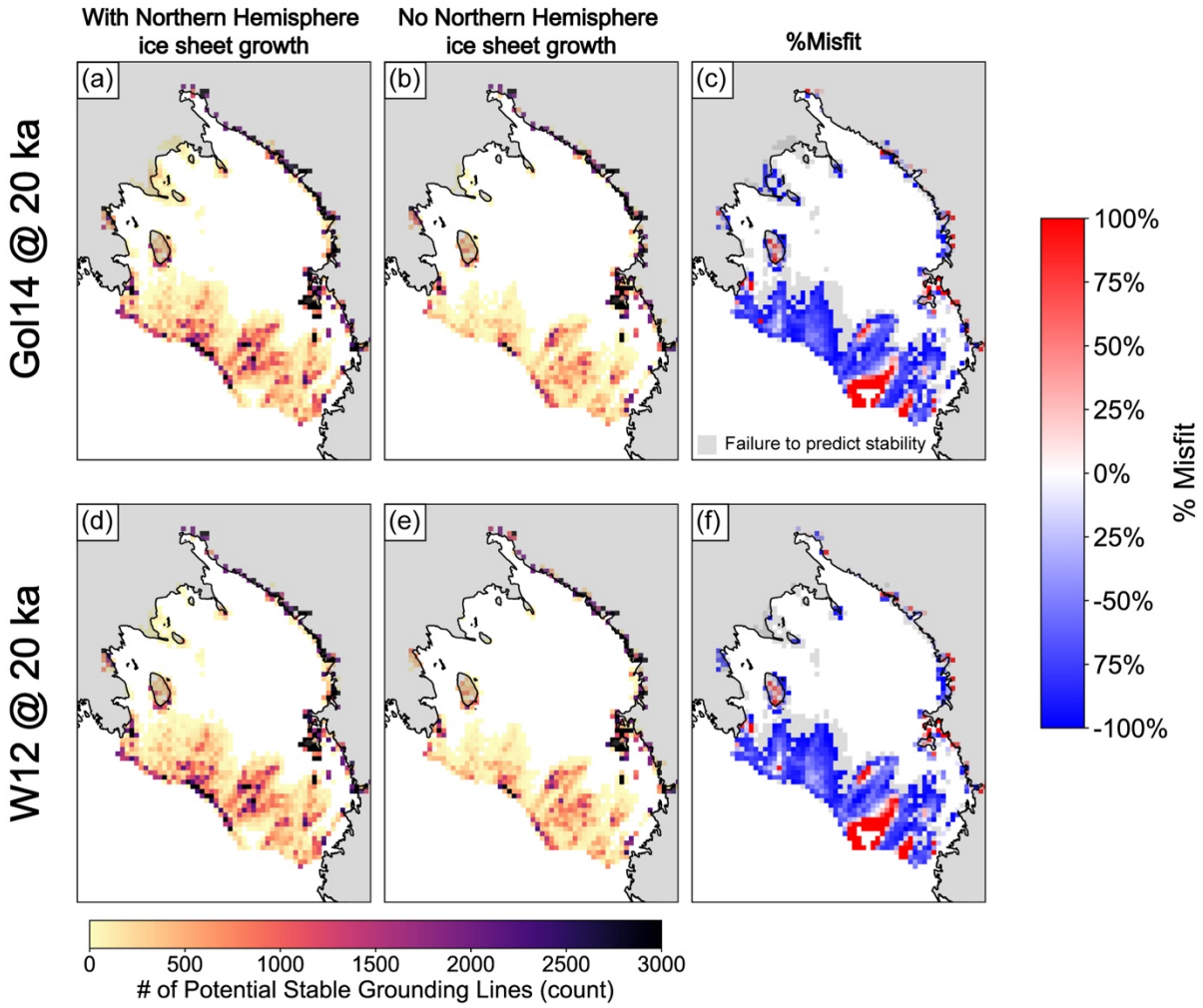

Figure S4 | Zones of potential persistence (ZPP) for Gol14 ice history at 20 ka a) including Northern Hemisphere (NH) ice sheets b) excluding Northern Hemisphere ice sheets c) Percent misfit defined as difference of stable grounding line positions calculated with NH ice sheets and no NH ice sheets divided by stable grounding line positions calculated using NH ice sheets $\left(\frac{ZPP_{NH}-ZPP_{no\ NH}}{ZPP_{NH}}\right)$. d-f) same as a-c) but with the W12 ice history.

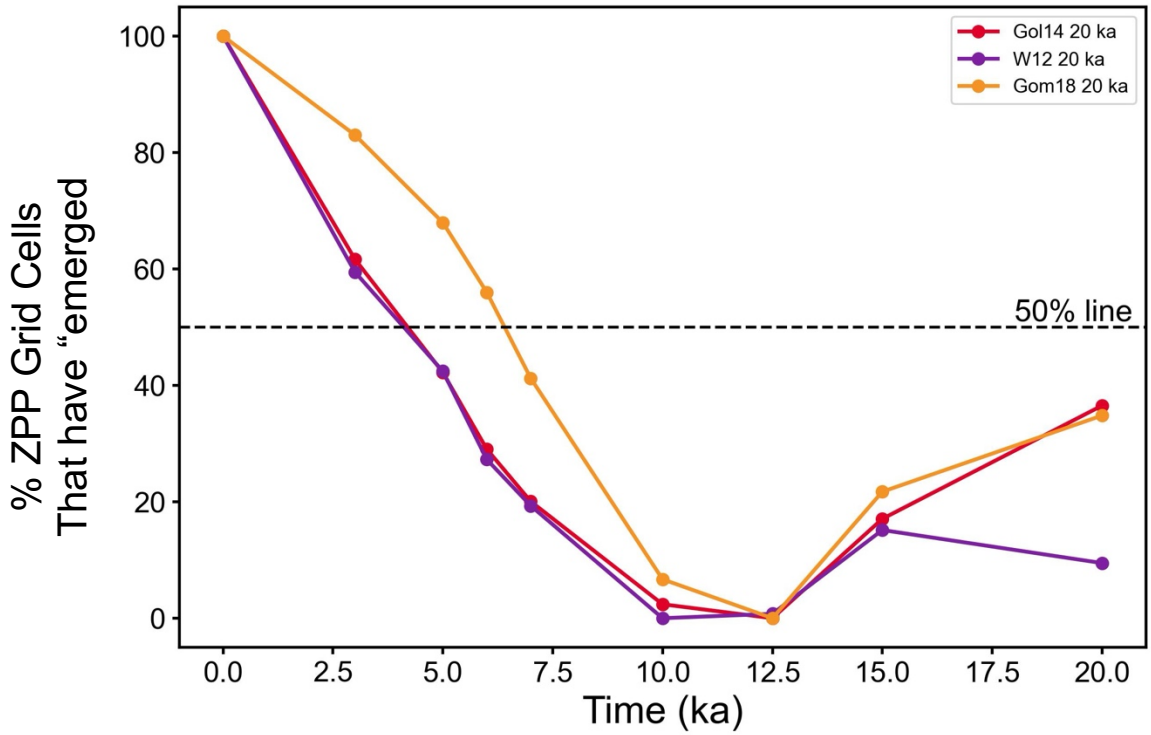

Figure S5 | Percent of "emergent" zones of potential persistence (zones that are stable at present-day but not stable in the past) that are stable at different times across the deglaciation. For each time-step we calculate the number of "emergent" zones of potential persistence (zones that are stable at present-day, but not stable at the current time-step), and then normalize by the maximum number of "emergent" zones of potential persistence across the whole deglaciation. Dashed line denotes 50%.

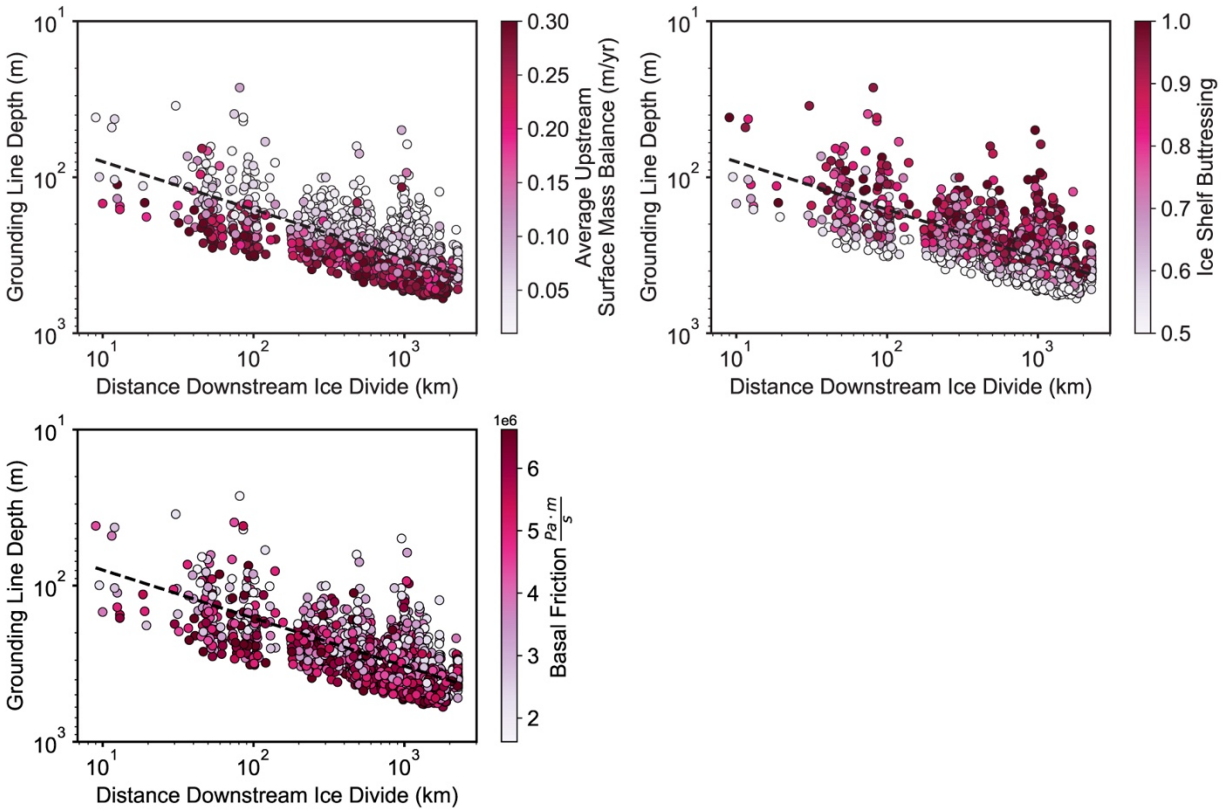

Figure S6 | Grounding line depth plotted as a function of distance downstream from the ice divide for our stability analysis ensemble. Points are colored by a) average accumulation rate, b) ice shelf buttressing coefficient, and c) basal friction coefficient.

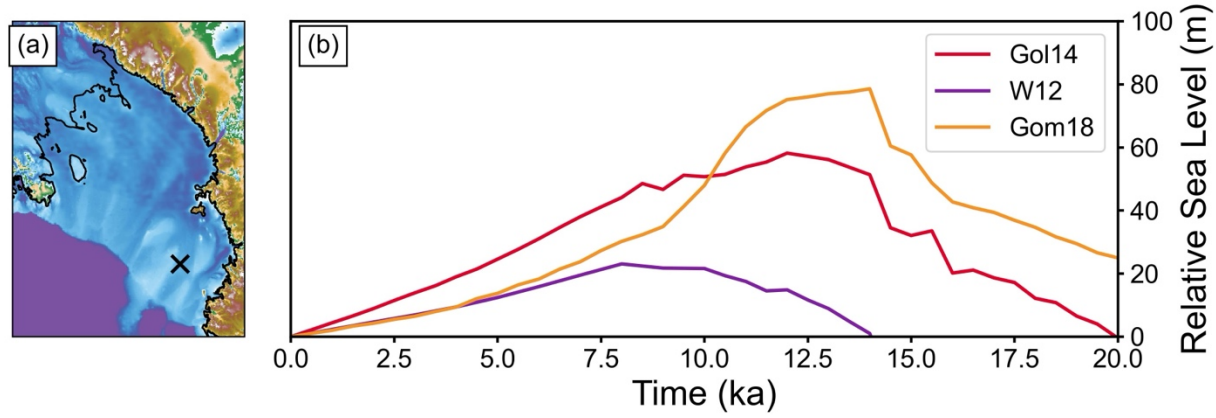

Figure S7 | a) Location of relative sea-level history in b) Relative sea level history over the past 20 ka for the Gol14 (red), W12 (purple), and Gom18 (orange) ice histories. Relative Sea-level fall due to isostatic rebound may have placed a role in the changes in flow direction and readvance during the Holocene (Greenwood et al., 2018; Lee et al., 2017).

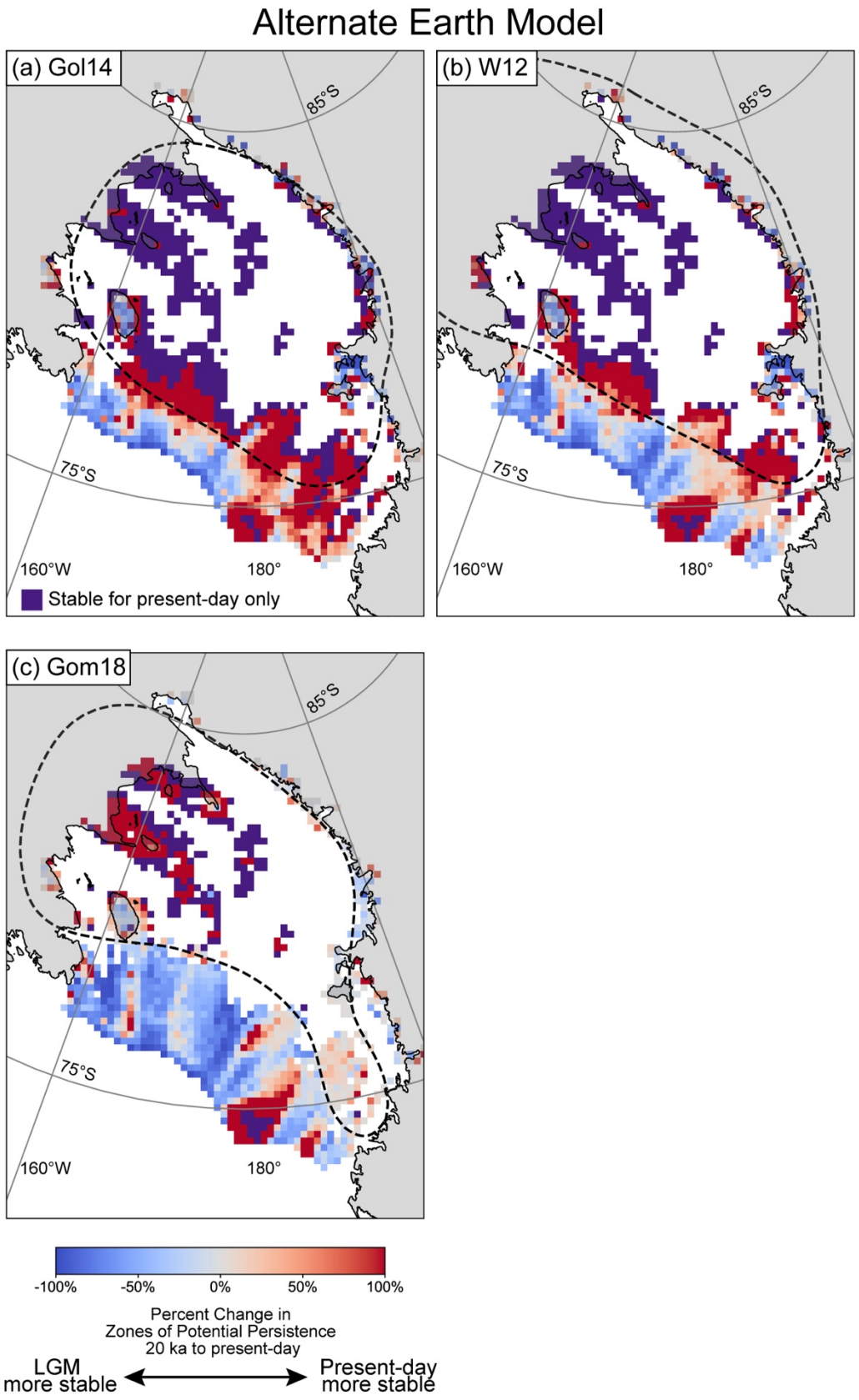
Alternate Earth Model
(a) Gol14
(b) W12
(c) Gom18
85°S
75°S
160°W
180°
Stable for present-day only
-100%
-50%
0%
50%
100%
Percent Change in
Zones of Potential Persistence
20 ka to present-day
LGM
more stable
Present-day
more stable

Figure S8| Change in zones of potential persistence across 20 km x 20 km grid cells based on glacial isostatic adjustment simulations using alternate Earth model for a) Gol14, b) W12, (50 km lithosphere and low viscosity zone of 10^{19} Pa·s from 50 km to 200 km depth, viscosity of 0.2 x 10^{21} Pa·s from 200 km to 670 km depth, and lower mantle viscosity of 3 x 10^{21} Pa·s) and c) Gom18 (see Gomez et al., 2018 for differences). Grid cells that have stable grounding line positions in the present-day and no stable grounding line positions at 20 ka ("emergent") are colored in purple. Thin black line is present-day day grounding line.

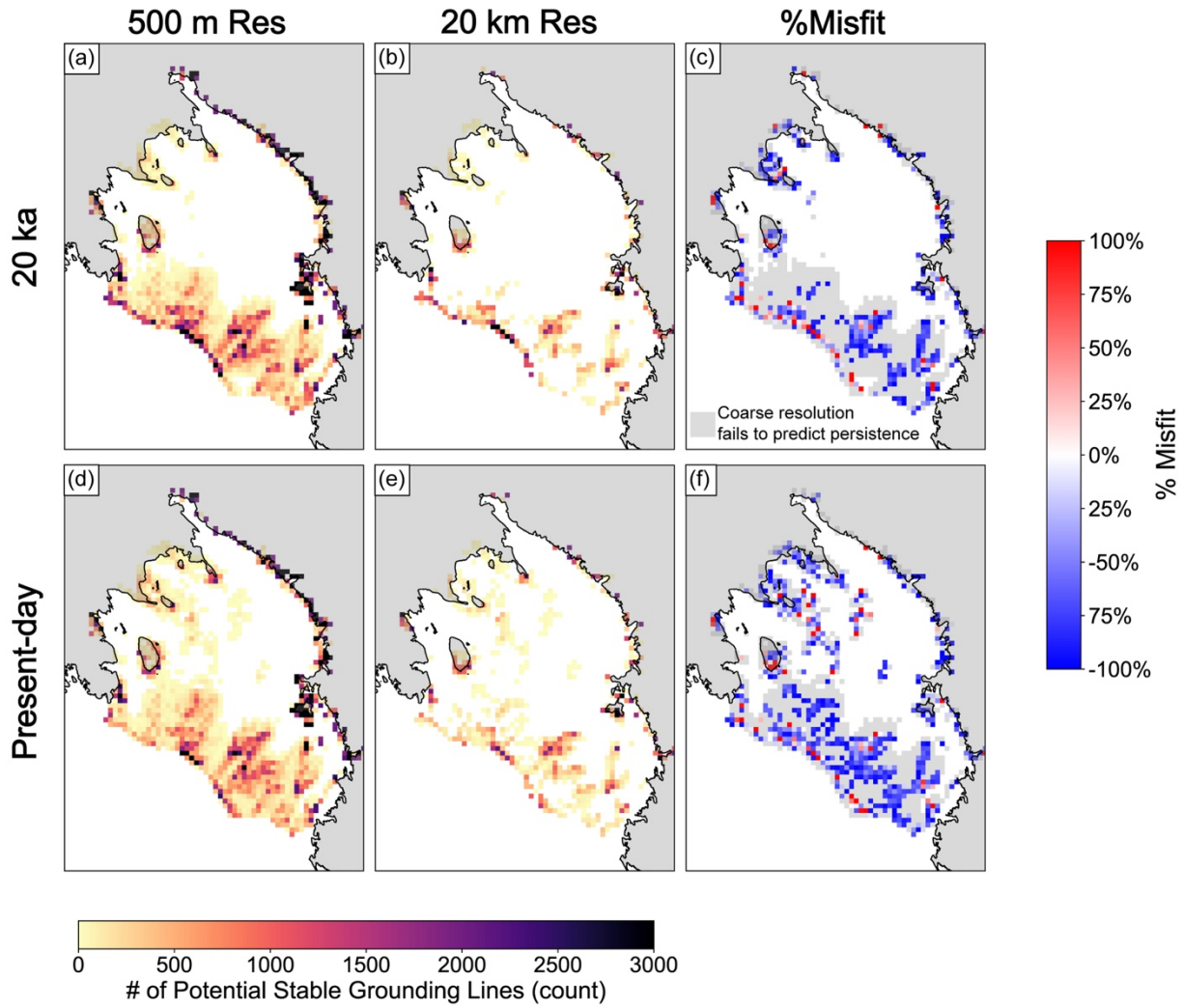

Figure S9 | Zones of potential persistence for Gol14 Last Glacial Maximum (20 ka) (top row), Present-day (bottom row) for high resolution (50m; a/d) and low resolution (20 km; b/e) Percent misfit for 20 ka (c) and present-day (f), defined as difference of zones of potential persistence calculated using high resolution and coarse resolution bathymetry divided by zones of potential persistence calculated using high resolution bathymetry $\left(\frac{ZPP_{500m}-ZPP_{20km}}{ZPP_{500m}}\right)$. Light grey shows where coarse resolution fails to predict persistence.

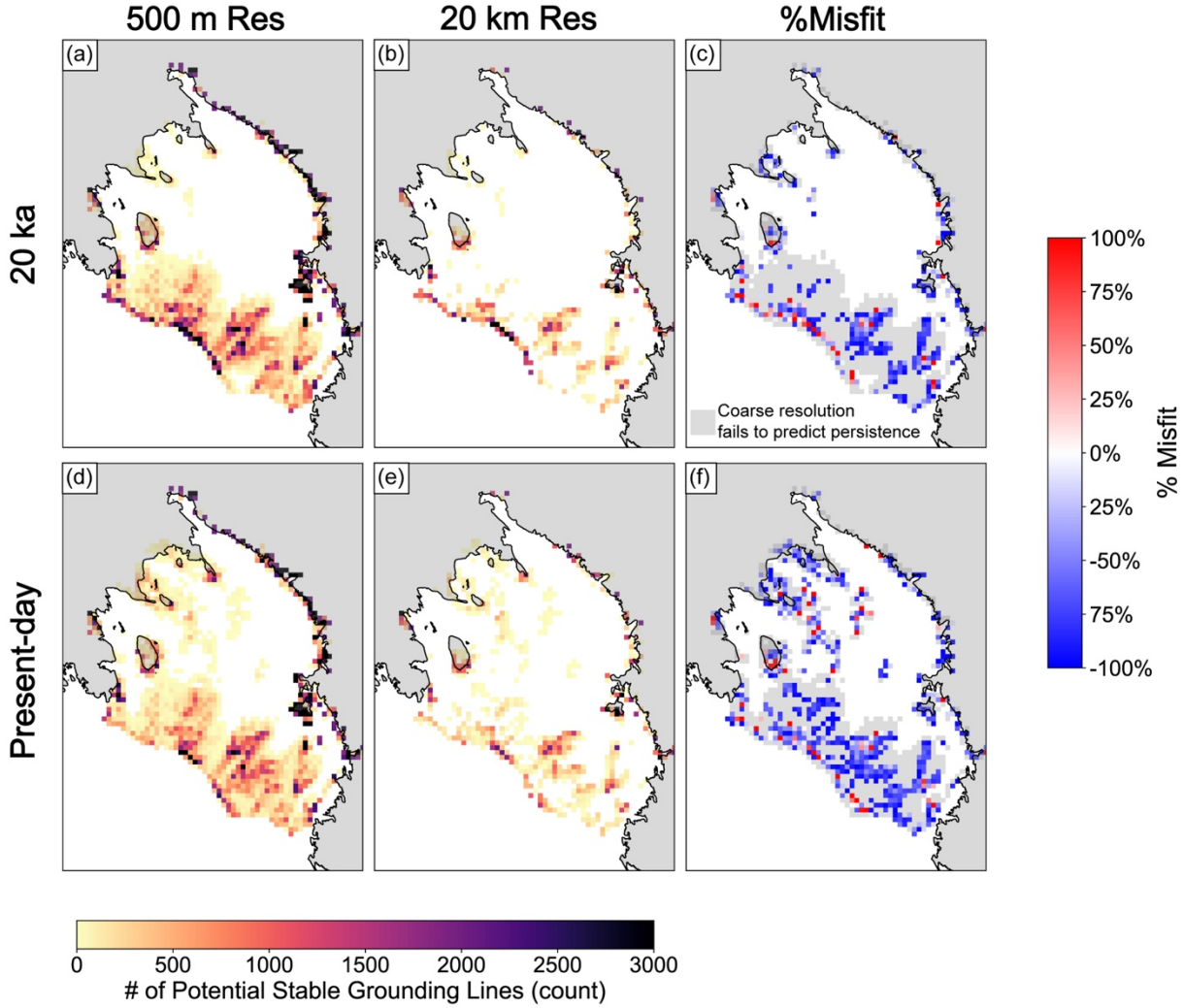

Figure S10 | Figure S9 | Same as main text Figure 5 but for W12. Zones of potential persistence for W12 Last Glacial Maximum (20 ka) (top row), Present-day (bottom row) for high resolution (50m; a/d) and low resolution (20 km; b/e) Percent misfit for 20 ka (c) and present-day (f), defined as difference of zones of potential persistence calculated using high resolution and coarse resolution bathymetry divided by zones of potential persistence calculated using high resolution bathymetry $\left(\frac{ZPP_{500m}-ZPP_{20km}}{ZPP_{500m}}\right)$. Light grey shows where coarse resolution fails to predict persistence.

References

Golledge, N. R., Menviel, L., Carter, L., Fogwill, C. J., England, M. H., Cortese, G., and Levy, R. H.: Antarctic contribution to meltwater pulse 1A from reduced Southern Ocean overturning, Nature Communications, 5, https://doi.org/10.1038/ncomms6107, 2014.

Gomez, N., Latychev, K., and Pollard, D.: A coupled ice sheet-sea level model incorporating 3D earth structure: Variations in Antarctica during the Last Deglacial Retreat, Journal of Climate, 31, 4041–4054, https://doi.org/10.1175/JCLI-D-17-0352.1, 2018.

Rignot, E., Mouginot, J., and Scheuchl, B.: Ice Flow of the Antarctic Ice Sheet, Science, 333, 1427–1430, https://doi.org/10.1126/science.1208336, 2011.

Robel, A., A.: SSAsimpleM, 2021.

Schoof, C.: Ice sheet grounding line dynamics: Steady states, stability, and hysteresis, Journal of Geophysical Research: Earth Surface, 112, https://doi.org/10.1029/2006JF000664, 2007.

Whitehouse, P. L., Bentley, M. J., and Le Brocq, A. M.: A deglacial model for Antarctica: Geological constraints and glaciological modelling as a basis for a new model of Antarctic glacial isostatic adjustment, Quaternary Science Reviews, 32, 1–24, https://doi.org/10.1016/j.quascirev.2011.11.016, 2012.